Available online at www.sciencedirect.com
ScienceDirect
Applied Catalysis B: Environmental 82 (2008) 103–113
APPLIED CATALYSIS B: ENVIRONMENTAL
www.elsevier.com/locate/apcatb

Kinetic dependencies and reaction pathways in hydrocarbon and oxyhydrocarbon conversions catalyzed by ceria-based materials

N. Laosiripojana [a,*], S. Assabumrungrat [b]

[a] *The Joint Graduate School of Energy and Environment, King Mongkut's University of Technology Thonburi, Bangkok 10140, Thailand*
[b] *Center of Excellence on Catalysis and Catalytic Reaction Engineering, Department of Chemical Engineering, Chulalongkorn University, Bangkok 10330 Thailand*

Received 8 February 2007; received in revised form 8 January 2008; accepted 16 January 2008
Available online 20 January 2008

Abstract

Hydrocarbons (i.e. CH_4, C_2H_4, C_2H_6, and C_3H_8) and oxyhydrocarbon (i.e. CH_3OH) conversions with and without co-reactants (H_2O and CO_2) were studied over ceria-based materials prepared by precipitation and cationic surfactant-assisted methods with/without Zr doping with an aim to understand their influences on material specific surface area, oxygen storage capacity (OSC), hydrocarbon reaction rate, resistance toward carbon deposition, and rigorous kinetic dependencies.

High surface area CeO_2 and Ce-ZrO_2 from the cationic surfactant-assisted method provided a higher degree of oxygen storage capacity (OSC) and reaction rates with greater resistance toward carbon deposition than those from the precipitation method. The reaction rates (mol g_{cat}^{-1} s^{-1}) per degree of OSC (mol$_{Oxygen}$ g_{cat}^{-1}) were identical for all materials, indicating the linear influence of OSC on the rates. Nevertheless, the kinetic dependencies were unaffected by specific surface area, doping element, degree of OSC and reactions (i.e. H_2O reforming, CO_2 reforming and cracking). The rates were proportional to hydrocarbon partial pressures with positive fraction reaction orders; independent of co-reactant partial pressures; but inhibited by CO and H_2. These kinetic dependencies were explained by a set of redox mechanistic proposal, in which the relevant elementary step is the reaction of intermediate surface hydrocarbon with lattice oxygen (O_O^x), and that lattice oxygen is efficiently replenished by rapid surface reactions with oxygen source from either CO_2, H_2O, or even CH_3OH.

Keywords: Ceria; Oxygen storage capacity; Reforming; Redox mechanistic; Kinetic

1. Introduction

Cerium oxide (or ceria) based material contains a high concentration of mobile oxygen vacancies, which act as local sources or sinks for oxygen involved in reactions taking place on its surface. The high oxygen mobility and oxygen storage capacity render this material very interesting for a wide range of catalytic applications involving oxidation and reforming of hydrocarbons [1–8]. Recently, one of the great potential applications of ceria-based materials is in an Indirect Internal Reforming-Solid Oxide Fuel Cell (IIR-SOFC) as an in-stack reforming catalyst [9,10]. In addition, it is also successfully applied in a direct internal reforming (DIR-SOFC), in which hydrocarbon and oxyhydrocarbon compounds (i.e. C_4H_{10} and CH_3OH) were efficiently reformed at ceria-based anodes (i.e. Cu-CeO_2 and Cu-CeO_2-YSZ) [11–16].

It has been well established that the gas–solid reaction between hydrocarbons and the lattice oxygen (O_x^o) on ceria surface can generate CO and H_2 at high temperature; in addition, the reactions of reduced ceria with oxygen-containing reactants, i.e. CO_2 and H_2O can regenerate the lattice oxygen (O_x^o) on CeO_2 surface [10,17–19]. The great benefit of ceria-based catalysts for reforming reactions is their high resistance toward carbon deposition compared to conventional metal catalysts [9,10]; however, the weaknesses are their low specific surface area and high deactivation due to the thermal sintering particularly when operated at such a high temperature [20]. The use of high surface area ceria (CeO_2 (HSA)) with high resistance toward the sintering was proposed to be a good approach to improve its catalytic reactivity [20]. Several techniques have been described for the preparation of CeO_2 (HSA) solid solution, i.e. homogeneous precipitation techni-

* Corresponding author. Tel.: +66 2 8729014; fax: +66 2 8726736.
E-mail address: navadol_l@jgsee.kmutt.ac.th (N. Laosiripojana).

0926-3373/$ – see front matter © 2008 Elsevier B.V. All rights reserved.
doi:10.1016/j.apcatb.2008.01.009

ques with precipitating agents and additives [21–24], hydrothermal synthesis [25], spray pyrolysis methods [26], inert gas condensation of Ce followed by oxidation [27], thermal decomposition of carbonates [28], microemulsion [29], and electrochemical methods [30]. However, a few of these composites showed regular pore structure after calcination at moderate temperatures and a severe loss of surface area occurs during the thermal treatment [31]. Recently, Terribile et al. [32] synthesized CeO_2 (HSA) with improved textural, structural and chemical properties by using a novel cationic surfactant-assisted approach. They reported that CeO_2 with surface area of 40 $m^2\ g^{-1}$ was achieved after calcination at 1173 K. Compared to conventional CeO_2 (CeO_2 (LSA)) prepared by precipitation technique with surface area less than 10 $m^2\ g^{-1}$ after calcination at 1173 K [10], this highlights the great potential of CeO_2 prepared by surfactant-assisted technique for application as a catalyst under high reaction temperature. It should be noted that, apart from the investigation on preparation method, the addition of zirconium oxide (ZrO_2) has also been widely reported to improve surface area, oxygen storage capacity, redox property, thermal stability and catalytic activity of ceria [33–39].

Focusing on the reforming reactions of hydrocarbon compounds over ceria-based materials, until now, the reaction pathways and kinetic dependencies remains unclear. Here, we thereby probe the kinetic dependencies of hydrocarbons (i.e. CH_4, C_2H_4, C_2H_6, and C_3H_8) and also oxyhydrocarbon (i.e. CH_3OH) conversion with and without co-reactants over ceria-based materials prepared by precipitation and cationic surfactant-assisted methods and with/without Zr doping. The relation between the material specific surface area, doping element, oxygen storage capacity (OSC), reaction rate, resistance toward carbon deposition, and kinetic dependence were identified. A rigorous kinetic, reaction pathways and rate expressions were then established.

2. Experimental methods

2.1. Material synthesis and characterization

CeO_2 was synthesized by precipitation (CeO_2 (LSA)) and cationic surfactant-assisted (CeO_2 (HSA)) methods. These preparation methods were described elsewhere in our previous publication [40]. The materials were dried overnight in ambient air at 383 K, and then calcined in a flow of dry air by increasing the temperature to 1173 K with a rate of 0.167 $K\ s^{-1}$ and holding at 1173 K for 6 h. After calcined, fluorite-structured CeO_2 with good homogeneity were obtained.

$Ce_{1-x}Zr_xO_2$ (or Ce-ZrO_2) with different Ce/Zr molar ratios were prepared by either co-precipitation or surfactant-assisted method of cerium nitrate ($Ce(NO_3)_3{\cdot}H_2O$), and zirconium oxychloride ($ZrOCl_2{\cdot}H_2O$) (from Aldrich). The ratio between each metal salt was altered to achieve nominal Ce/Zr molar ratios: $Ce_{1-x}Zr_xO_2$, where x = 0.25, 0.50, and 0.75 respectively. After treatment, the specific surface areas of all CeO_2 and Ce-ZrO_2 were achieved from BET measurement. As presented in Table 1, after drying in the oven, surface areas of 105 and 55 $m^2\ g^{-1}$ were observed for CeO_2 (HSA) and CeO_2 (LSA), respectively and, as expected, the surface area decreased at high calcination temperatures. However, the value for CeO_2 (HSA) is still appreciable after calcination at 1173 K. It can also be seen that the introduction of ZrO_2 stabilizes the surface area of ceria, which is in good agreement with several previous reports [41–43]. After treatment, the degree of OSC and redox reversibilities of all CeO_2 and Ce-ZrO_2 were determined by the temperature programmed reduction (TPR-1) and temperature programmed oxidation (TPO) following with second time temperature programmed reduction (TPR-2), respectively, at the same conditions. Details of these measurements are given in Section 3.1.

Table 1
Specific surface areas of ceria-based materials before and after calcination at 1173 K

Catalysts	Surface area after drying ($m^2\ g^{-1}$)	Surface area after calcinations ($m^2\ g^{-1}$)
CeO_2 (HSA)	105	29
Ce-ZrO_2 (HSA) (Ce/Zr = 1/3)	135	49
Ce-ZrO_2 (HSA) (Ce/Zr = 1/1)	120	47
Ce-ZrO_2 (HSA) (Ce/Zr = 3/1)	115	46.5
CeO_2 (LSA)	55	11
Ce-ZrO_2 (LSA) (Ce/Zr = 1/3)	82	22
Ce-ZrO_2 (LSA) (Ce/Zr = 1/1)	74	20.5
Ce-ZrO_2 (LSA) (Ce/Zr = 3/1)	70	20

2.2. Catalytic H_2O and CO_2 reforming and cracking of hydrocarbons

To undergo the catalytic testing, an experimental reactor system was constructed as shown elsewhere [40]. The feed gases including the components of interest, i.e. CH_4, C_2H_4, C_2H_6, C_3H_8, CH_3OH, deionized H_2O (introduced via a syringe pump pass through an evaporator), CO_2, CO, and H_2 were introduced to a 10-mm diameter quartz reactor, which was mounted vertically inside tubular furnace. The catalysts (50 mg of ceria-based catalysts) were diluted with SiC (to obtain the total weight of 500 mg) in order to avoid temperature gradients and loaded in the quartz reactor. Preliminary experiments were carried out to find suitable conditions in which internal and external mass transfer effects are not predominant. Considering the effect of external mass transfer, the total flow rate was kept constant at 100 $cm^3\ min^{-1}$ under a constant residence time of 5×10^{-3} g min cm^{-3} in all testing. The suitable average sizes of catalysts were also verified in order to confirm that the experiments were carried out within the region of isothermal kinetics. In our system, a Type-K thermocouple was placed into the annular space between the reactor and furnace. This thermocouple was mounted in close contact with the catalyst bed to minimize the temperature difference. Another Type-K thermocouple, covering by closed-end quartz tube, was inserted in the middle of the quartz reactor in order to re-check the possible temperature gradient.

Table 2
Results of TPR-1, TPO, TPR-2 analyses of ceria-based materials after calcination

Catalyst	Total H_2 uptake from TPR-1 ($\mu mol/g_{cat}$)	Total O_2 uptake from TPO ($\mu mol/g_{cat}$)	Total H_2 uptake from TPR-2 ($\mu mol/g_{cat}$)
CeO_2 (HSA)	4105	2067	4109
Ce-ZrO_2 (HSA) (Ce/Zr = 1/3)	2899	1475	2876
Ce-ZrO_2 (HSA) (Ce/Zr = 1/1)	3701	1862	3694
Ce-ZrO_2 (HSA) (Ce/Zr = 3/1)	5247	2640	5250
CeO_2 (LSA)	1794	898	1788
Ce-ZrO_2 (LSA) (Ce/Zr = 1/3)	1097	553	1085
Ce-ZrO_2 (LSA) (Ce/Zr = 1/1)	1745	744	1746
Ce-ZrO_2 (LSA) (Ce/Zr = 3/1)	2649	1328	2643

After the reactions, the exit gas mixture was transferred via trace-heated lines (373 K) to the analysis section, which consists of an online Porapak Q column Shimadzu 14B gas chromatograph (GC) with TCD and FID detectors and a mass spectrometer (MS). The GC was applied for the steady state kinetic studies, whereas the MS in which the sampling of the exit gas was done by a quartz capillary and differential pumping was used for the transient experiments. Kinetic effects were studied over wide ranges of temperature and reactant partial pressures.

2.3. Measurement of carbon formation

The temperature programmed oxidation (TPO) was applied to investigate the amount of carbon formed on catalyst surface by introducing 10% O_2 in He into the system, after purging with helium. The operating temperature increased from room temperature to 1273 K by a rate of 10 K min^{-1}. The amount of carbon formation on the surface of catalysts was determined by measuring the CO and CO_2 yields from the TPO results. In addition to the TPO method, the amount of carbon deposition was reconfirmed by the calculation of carbon balance in the system, which theoretically equals to the difference between inlet and outlet carbon containing components.

3. Results and discussion

3.1. Redox properties and redox reversibility

After treatment, the degree of OSC for fresh ceria-based materials were investigated using TPR-1, which was performed by heating the catalysts up to 1273 K in 5%H_2 in He. The amount of H_2 uptake was correlated to the amount of oxygen stored in the catalysts. As presented in Table 2, the amount of H_2 uptakes over Ce-ZrO_2 and CeO_2 (HSA) are significantly higher than those over the low surface area cerias, suggesting the increasing of OSC with the doping of Zr and the increasing of material specific surface area. The benefit of OSC on the reforming reaction will be later presented in Section 3.3.

After purging with He, the redox reversibilities were then determined by applying TPO following with TPR-2. The TPO was carried out by heating the catalyst up to 1273 K in 10%O_2 in He; the amounts of O_2 chemisorbed were then measured, Table 2. Regarding the TPR-2 results as also shown in Table 2, the amount of hydrogen uptakes for all materials were approximately similar to those from the TPR-1, indicating the reversibility of OSC for these synthesized ceria-based materials.

3.2. Reactivity toward the (H_2O and CO_2) reforming and cracking of CH_4

The H_2O reforming, CO_2 reforming and cracking of CH_4 were tested at 1123 K by introducing CH_4 along with co-reactant (for H_2O and CO_2 reforming). It should be noted that the reactions over Ce-ZrO_2 catalysts with different Ce/Zr ratios (1/3, 1/1, and 3/1) were firstly tested. The results revealed that Ce-ZrO_2 with Ce/Zr ratio of 3/1 shows the best performance in terms of stability and activity. Therefore, we report here detailed reactivity and kinetic data of Ce-ZrO_2 only with Ce/Zr ratio of 3/1.

Fig. 1 shows the variations in CH_4 reforming rate ($mol_{CH_4}\, g_{cat}^{-1}\, s^{-1}$) with time at the initial state (10 min; using MS) over Ce-ZrO_2 (HSA) by varying inlet co-reactant/CH_4 ratios from 0.0 (cracking reaction) to 0.3, 0.5, 0.7, 1.0, and 2.0, while Fig. 2 shows the stability and activity (under the period of 10 h; using GC-TCD) of H_2O and CO_2 reforming of CH_4 over several catalysts. The reforming rates expressed in the figures are obtained from the relation between the measured net reaction rate (r_m; $mol_{CH_4}\, g_{cat}^{-1}\, s^{-1}$) and the approach to equilibrium condition (η) using the following equation [44]:

$$r_t = r_m(1-\eta)^{-1} \tag{1}$$

where η is either the approach to equilibrium for H_2O reforming (η_s) or for CO_2 reforming (η_d). Both parameters are determined from the following equation:

$$\eta_s = \frac{[P_{CO}][P_{H_2}]^3}{[P_{CH_4}][P_{H_2O}]}\frac{1}{K_s} \tag{2}$$

$$\eta_d = \frac{[P_{CO}]^2[P_{H_2}]^2}{[P_{CH_4}][P_{CO_2}]}\frac{1}{K_d} \tag{3}$$

where P_i is partial pressure of component i (atm); K_s and K_d are the equilibrium constants for H_2O and CO_2 reforming of CH_4 at a given temperature. It should be noted that, in the present work, the values of η were always kept below 0.2 in all experiments.

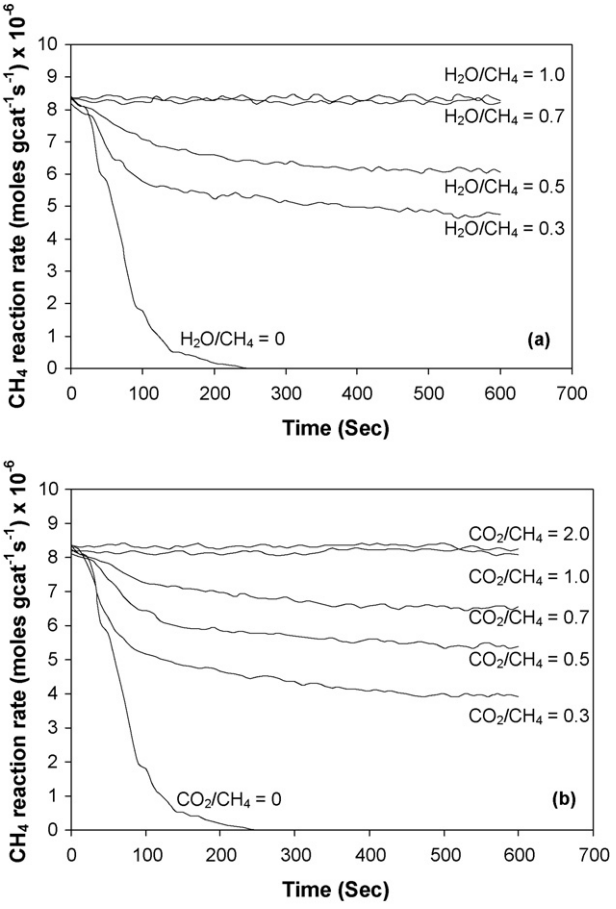

Fig. 1. CH_4 reaction rate at initial state (10 min) for H_2O reforming of CH_4 (a) and CO_2 reforming of CH_4 (b) over Ce-ZrO_2 (HSA) (1123 K with 3 kPa CH_4 in He).

The main products from the reactions over these catalysts were H_2 and CO with some CO_2, indicating a contribution from the water–gas shift at this high temperature. Based on the measured concentrations of reactants and products during CH_4 reforming, the approach to water-gas shift equilibrium condition (η_{WGS}) in the range of temperature studied (1023–1123 K) are always close to 1.0 in all type of catalysts, indicating that water–gas shift (WGS) reaction is at equilibrium. Fig. 1 indicates that the initial CH_4 reforming rate is unaffected by the concentration and type of co-reactants. Nevertheless, significant deactivation was observed for the cracking of CH_4 due to the loss of lattice oxygen (O_O^x) on the surface of ceria-based materials without the replacement by external oxygen containing sources (i.e. H_2O and CO_2). The rate of deactivation rapidly reduced when small content of H_2O or CO_2 was added.

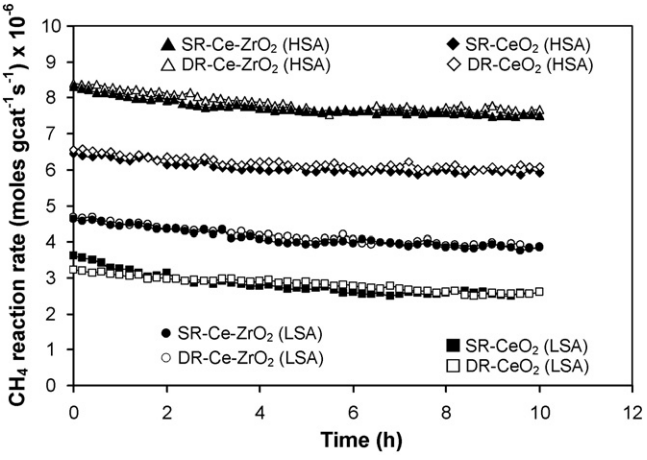

Fig. 2. Stability and activity testing of H_2O reforming (SR) and CO_2 reforming (DR) of CH_4 over several catalysts (at 1123 K with 3 kPa CH_4 and 3 kPa co-reactants).

Fig. 2 indicates that, at steady state, the high surface area materials showed much higher reactivity toward the CH_4 reforming than the low surface area one. Nevertheless, it should be noted that the CH_4 reaction rates ($mol_{CH_4}\ g_{cat}^{-1}\ s^{-1}$) per surface area ($m^2\ g^{-1}$) (in Table 1) for each type of catalyst with different surface areas are in the same range, e.g. $2.0-2.2 \times 10^{-7}\ mol_{CH_4}$ $(m^2\ s)^{-1}$ for CeO_2, $1.0-1.1 \times 10^{-7}\ mol_{CH_4}$ $(m^2\ s)^{-1}$ for Ce-ZrO_2 (Ce/Zr = 1/1), and $1.6-1.8 \times 10^{-7}\ mol_{CH_4}$ $(m^2\ s)^{-1}$ for Ce-ZrO_2 (Ce/Zr = 3/1) (with the operating conditions of 3 kPa CH_4 at 1123 K) indicating the great impact of catalyst specific surface area on the rate. In addition, importantly, at the same reaction conditions, the CH_4 reaction rates ($mol_{CH_4}\ g_{cat}^{-1}\ s^{-1}$) per degree of OSC ($mol_{Oxygen}\ g_{cat}^{-1}$) (in Table 2) for all catalyst are approximately identical ($2.8 \times 10^{-3}\ mol_{CH_4}\ mol_{oxygen}^{-1}\ s^{-1}$ for the inlet CH_4 of 3 kPa at 1123 K) indicating the linear influence of OSC on the reforming reactivity.

After purging in helium, the TPO detected small amount of carbon on the surface of materials from CH_4 cracking reaction (between 0.09 and 0.15 mmol g_{cat}^{-1} for high surface area materials and between 0.18 and 0.21 mmol g_{cat}^{-1} for low surface area one). These amounts of carbon deposited were ensured by the calculation of carbon balance. Regarding the calculation, the moles of carbon remaining in the system were 0.07–0.14 mmol g_{cat}^{-1} for high surface area materials and were 0.20 ± 0.01 mmol g_{cat}^{-1} for low surface area materials, which are in good agreement with the values observed from the TPO. No carbon formation was observed on high surface area materials when the inlet H_2O/CH_4 and CO_2/CH_4 ratios were higher than 0.7 and 1.0, whereas low surface area materials required inlet H_2O/CH_4 and CO_2/CH_4 ratios higher than 1.0 and 2.0 to operate without detectable carbon. The good resistance toward carbon deposition for ceria-based materials, which has been widely reported by previous researchers [9–10], is mainly due to their sufficient oxygen storage capacity (OSC). It should be noted that we observed high amount of carbon formation on the surface of Ni catalysts after exposure in the same reforming conditions as ceria-based materials [45,46]. Regarding the possible carbon formation during the reforming processes, the following reactions are theoretically the most probable reactions that could lead to carbon formation:

$$2CO \Leftrightarrow CO_2 + C \quad (4)$$

$$CH_4 \Leftrightarrow 2H_2 + C \quad (5)$$

$$CO + H_2 \Leftrightarrow H_2O + C \quad (6)$$

$$CO_2 + 2H_2 \Leftrightarrow 2H_2O + C \quad (7)$$

At low temperature, reactions (6) and (7) are favorable, while reactions (4) and (5) are thermodynamically unflavored [47]. The Boudouard reaction (Eq. (4)) and the decomposition of CH_4 (Eq. (5)) are the major pathways for carbon formation at such a high temperature as they show the largest changes in Gibbs energy [48]. According to the range of temperature in this study, carbon formation would be formed via the decomposition of CH_4 and Boudouard reactions especially at high inlet CH_4/co-reactant ratio. By applying CeO_2, both reactions (Eqs. (4) and (5)) could be inhibited by the redox reaction between the surface carbon (C) forming via the adsorptions of CH_4 and CO (produced during the reforming process) with the lattice oxygen (O_O^x) at CeO_2 surface (Eq. (8)).

$$C + O_O^x \rightarrow CO + V_O^{\bullet\bullet} + 2e' \quad (8)$$

Using the Kroger–Vink notation, $V_O^{\bullet\bullet}$ denotes as an oxygen vacancy with an effective charge 2^+, and e' is an electron which can either be more or less localized on a cerium ion or delocalized in a conduction band. The greater resistance toward carbon deposition for high surface area ceria-based catalyst particularly Ce-ZrO_2 (HSA) is due to the significant higher amount of lattice oxygen (O_O^x) on their surfaces, according to the results in Section 3.1.

3.3. Kinetic dependencies of forward CH_4 reforming rate on partial pressures of reactants (i.e. CH_4 and H_2O or CO_2) and products (CO and H_2)

The kinetic dependencies of CH_4 reforming rates on the partial pressures of CH_4, H_2O, CO_2, CO, and H_2 for all ceria-based materials were studied in the temperature range of 1023–1123 K. All measurements were carried out under the operating conditions without detectable carbon formation by controlling H_2O/CH_4 and CO_2/CH_4 inlet ratios according to the results from Section 3.2.

Fig. 3 shows the effect of CH_4 partial pressure on the rate ($mol_{CH_4}\ mol_{oxygen}^{-1}\ s^{-1}$) over Ce-$ZrO_2$ (HSA) at several reaction temperatures, while Fig. 4 shows the effect of CH_4 partial pressure on the rate (per degree of OSC) over different catalysts

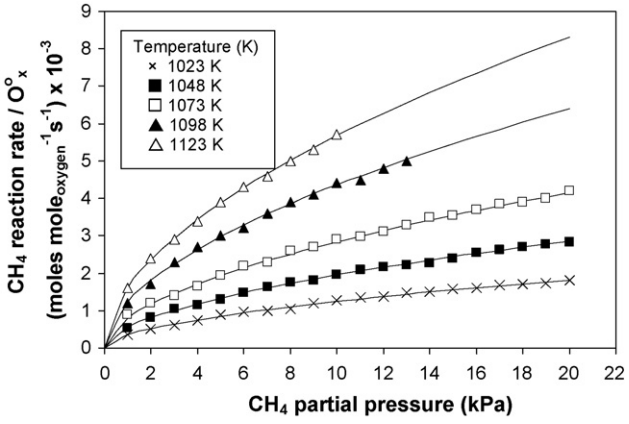

Fig. 3. Effect of temperature on CH_4 steam reforming over Ce-ZrO_2 (HSA) (with inlet CH_4/H_2O of 1.0).

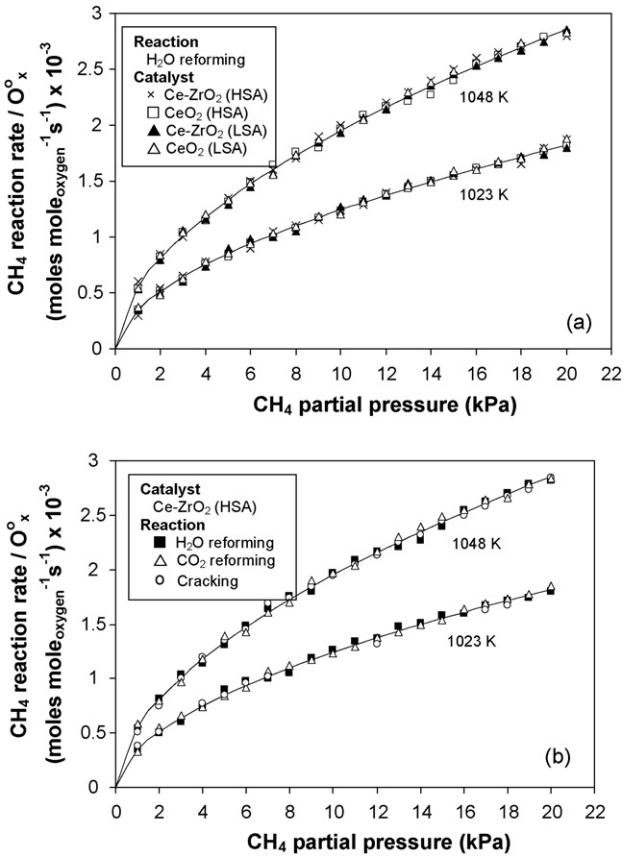

Fig. 4. Effect of CH_4 partial pressure on CH_4 reaction rate (per moles of oxygen stored) over different catalysts (a) and different reactions (b).

(Fig. 4a) and different reactions (i.e. H_2O reforming, CO_2 reforming and cracking (initial rates) of CH_4) (Fig. 4b). The rate increased with increasing CH_4 partial pressures and operating temperature for all catalysts and reactions. The reaction order in CH_4 was determined by plotting $\ln(r_t)$ versus $\ln \ln P_{CH_4}$ (the effects of product concentrations are taken into account via the term equilibrium condition (η)). The reaction orders in other components (CO_2, H_2O, H_2, and CO) were achieved using the same approach. The reaction order in CH_4 was observed to be positive fraction values approximately 0.52 ($\pm$0.03) for all catalysts and reactions, and seemed to be independent of temperature and co-reactant (CO_2 and H_2O) partial pressures in the range of conditions studied.

Several inlet CO_2 or H_2O partial pressures were then introduced to the feed with constant CH_4 partial pressure in order to investigate the influence of these co-reactant partial pressures on the rate. Fig. 5 shows the effects of co-reactant on CH_4 reaction rate with several inlet CH_4 partial pressures over different reactions (Fig. 5a) and over different catalysts (Fig. 5b). It is clear that the rates were not influenced by H_2O and CO_2 partial pressures; thus, the reaction orders in both components would be zero. The reforming in the presences of CO and H_2 were also investigated by adding either CO or H_2 to the feed gas at several operating temperatures. The results in Figs. 6 and 7 showed that the rates are dependent on both CO and H_2 concentrations. Unlike CH_4, both components inhibited the rate. The reaction order in CO was in the range of -0.15 to

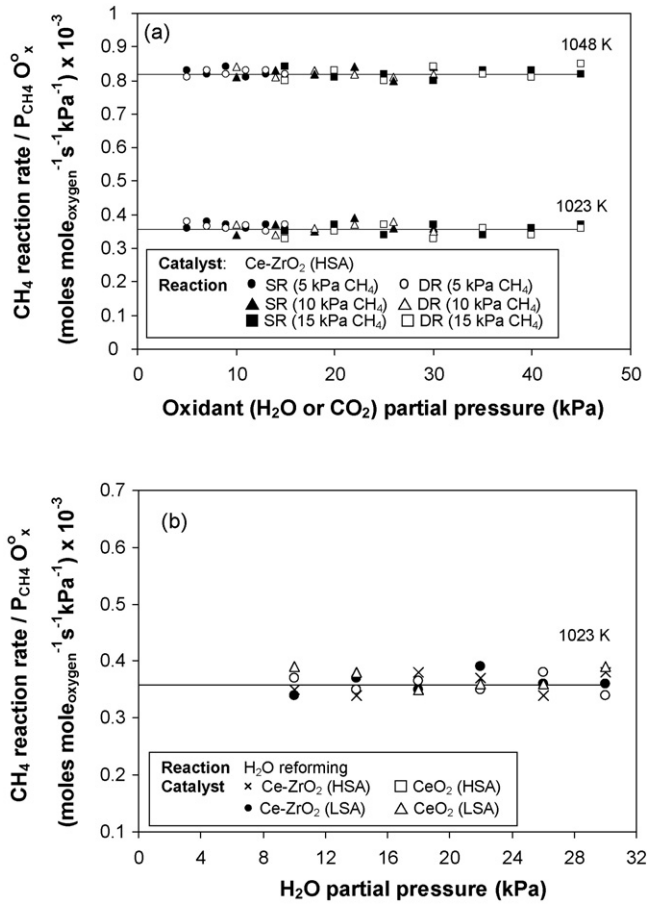

Fig. 5. Effect of co-reactant on CH_4 reaction rate (per moles of oxygen stored and inlet CH_4 partial pressure) over different reactions (with several inlet CH_4 partial pressures) (a) and different catalysts (b).

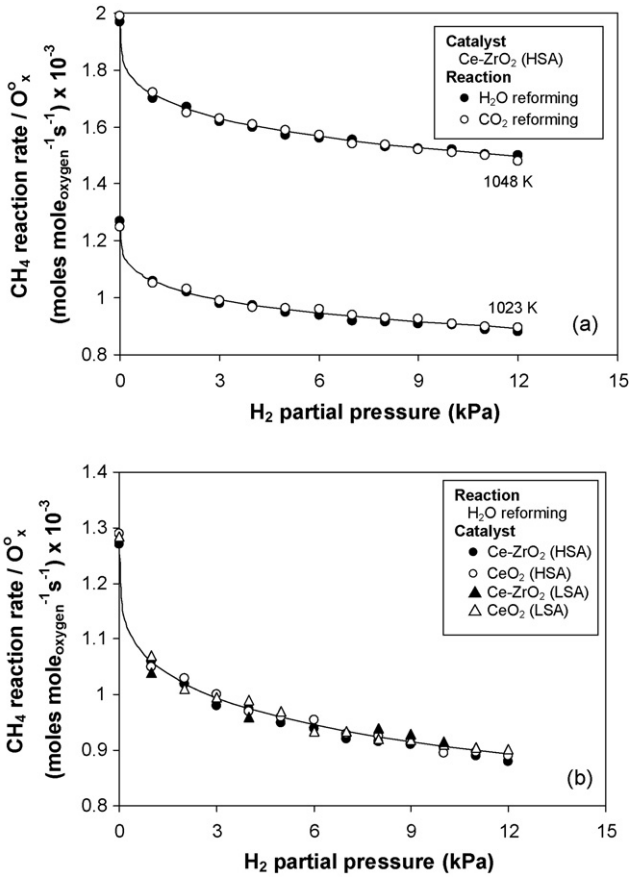

Fig. 6. Effect of H_2 on CH_4 reaction rate (per moles of oxygen stored) over different reactions (a) and different catalysts (b).

-0.12, while the reaction order in H_2 was between -0.31 and -0.28 for all catalysts. Similar reaction orders and kinetic constants for all ceria-based materials indicate that the kinetic dependencies are not affected by the specific surface area (or degree of OSC) and the doping of Zr.

Some previous researchers have proposed the redox mechanism to explain the reforming behavior of ceria-based catalysts [9,10]. They indicated that the reforming reaction mechanism involves the reaction between methane, or an intermediate surface hydrocarbon species, and lattice oxygen at the ceria-based material surface [9]. During reforming reaction, the isothermal reaction rate reaches steady state where the co-reactant, i.e. steam, provides a continuous source of oxygen. They also proposed that the controlling step is the reaction of methane with ceria, and that oxygen is replenished by a significantly more facile surface reaction of the ceria with steam [9]. Therefore, we suggested here that the CH_4 reaction pathway for ceria-based materials involves the reaction between absorbed CH_4 (forming intermediate surface hydrocarbon species) with the lattice oxygen (O_O^x) at CeO_2 surface, as illustrated schematically below.

CH_4 adsorption

$$CH_4 + 2* \rightarrow CH_3* + H* \quad (9)$$

$$CH_3* + * \rightarrow CH_2* + H* \quad (10)$$

$$CH_2* + * \rightarrow CH* + H* \quad (11)$$

$$CH* + * \rightarrow C* + H* \quad (12)$$

Co-reactant (H_2O and CO_2) adsorption

$$H_2O + 2* \Leftrightarrow OH* + H* \quad (13)$$

$$OH* + * \Leftrightarrow H* + O* \quad (14)$$

$$CO_2 + 2* \Leftrightarrow CO* + O* \quad (15)$$

Redox reactions of lattice oxygen (O_O^x) with C* and O*

$$C* + O_O^x \rightarrow CO* + V_O^{\bullet\bullet} + 2e' \quad (16)$$

$$V_O^{\bullet\bullet} + 2e' + O* \Leftrightarrow O_O^x + * \quad (17)$$

Inhibitory effects of CO and H_2

$$H_2 + 2* \Leftrightarrow H* + H* \quad (18)$$

$$H* + O_O^x \Leftrightarrow OH* + V_O^{\bullet\bullet} + 2e' \quad (19)$$

$$CO + * \Leftrightarrow CO* \quad (20)$$

$$CO* + O_O^x \Leftrightarrow CO_2* + V_O^{\bullet\bullet} + 2e' \quad (21)$$

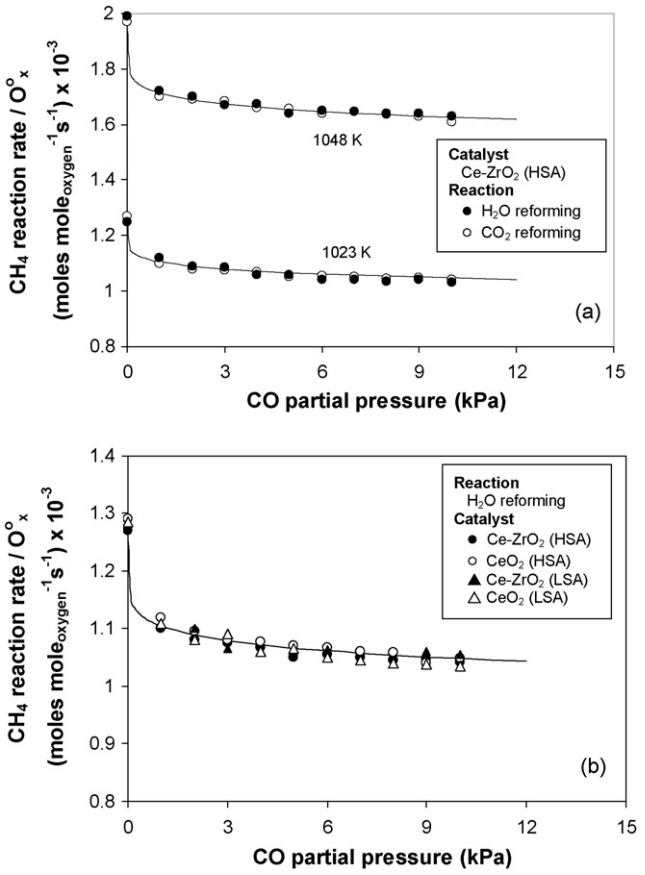

Fig. 7. Effect of CO on CH_4 reaction rate (per moles of oxygen stored) over different reactions (a) and different catalysts (b).

where * is the surface active site of ceria-based materials. During the reactions, CH_4 adsorbed on * forming intermediate surface hydrocarbon species (CH^*_x) (Eqs. (9–12)) and later reacted with the lattice oxygen (O_O^x) (Eq. (16)). The steady-state reforming rate is due to the continuous supply of the oxygen source by either CO_2 or H_2O (Eqs. (13–15)) that reacted with the reduced-state catalyst to recover lattice oxygen (O_O^x) (Eq. (17)). The identical rate for the H_2O and CO_2 reforming at similar CH_4 partial pressures, as well as the stronger linear dependence of the reforming rate on CH_4 partial pressure with the positive fraction value of reaction order in this component, and the independent effects of CO_2 and H_2O provide the evidence that the sole kinetically relevant elementary step is the reaction of intermediate surface hydrocarbon species with the lattice oxygen (O_O^x), and that oxygen is replenished by a significantly rapid surface reaction of the reduced state with the oxygen source from either CO_2 or H_2O; this fast step maintains the lattice oxygen (O_O^x) essentially unreduced by adsorbed intermediate surface hydrocarbon. The unchanged state of lattice oxygen was confirmed by the calculation of oxygen balance during reactions and TPO after reactions. We have used these methods to probe the state of lattice oxygen, because characterizations of used catalysts are not practical due to the low catalyst amounts used and its mixing with SiC. According to the oxygen balance calculation, the mole of oxygen (from co-reactant) fed into the system was almost similar to that in the products for all reactions and testing times indicating the unchanged state of CeO_2 (to CeO_{2-x}) during the experiments. Furthermore, the TPO results after reactions also proved the unchanged state of material, as no oxygen uptakes were detected.

The negative effects of CO and H_2 are due to the reactions between these adsorbed components (CO* and H*) with the lattice oxygen (O_O^x) (Eqs. (18–21)), which consequently result in the inhibition of CH_4 conversion. From all observation, a simple CH_4 reaction rate expression for H_2O reforming, CO_2 reforming and cracking (initial rate) can be written as following:

$$\text{Rate} = \frac{k[P_{CH_4}]^{0.5}}{1 + K_H[P_{H_2}]^{0.3} + K_{CO}[P_{CO}]^{0.15}} \quad (22)$$

where P_i is the partial pressure of chemical component i, k is the rate constant, and K_{CO} and K_H are adsorption parameters, obtained from Van't Hoff equation. The rate constants (k) and the activation energies measured from the H_2O reforming, CO_2 reforming and cracking (initial rate) of CH_4 are identical

Table 3
CH_4 reaction rate, rate constant and activation energies for CH_4 reactions on ceria-based materials (1048 K, 10 kPa CH_4 balance in He)

Catalysts	Reaction	CH_4 reaction rate/O_O^x (moles $mole^{-1}_{oxygen}$ s^{-1}) × 10^{-3}	Rate constant (s^{-1} kPa^{-1}) × 10^{-3}	Activation energy (kJ mol^{-1})
CeO_2 (HSA)	H_2O reforming	1.96	0.53	154.2
	CO_2 reforming	1.98	0.55	155.0
	Cracking	1.95[a]	0.53	151.8
Ce-ZrO_2 (HSA)	H_2O reforming	1.97	0.54	154.2
	CO_2 reforming	1.95	0.52	153.4
	Cracking	1.94	0.55	150.9
CeO_2 (LSA)	H_2O reforming	1.96	0.56	154.9
	CO_2 reforming	1.95	0.54	152.1
	Cracking	1.96	0.57	154.3
Ce-ZrO_2 (LSA)	H_2O reforming	1.95	0.56	155.2
	CO_2 reforming	1.94	0.55	154.4
	Cracking	1.97	0.55	153.2

[a] Initial CH_4 reaction rate.

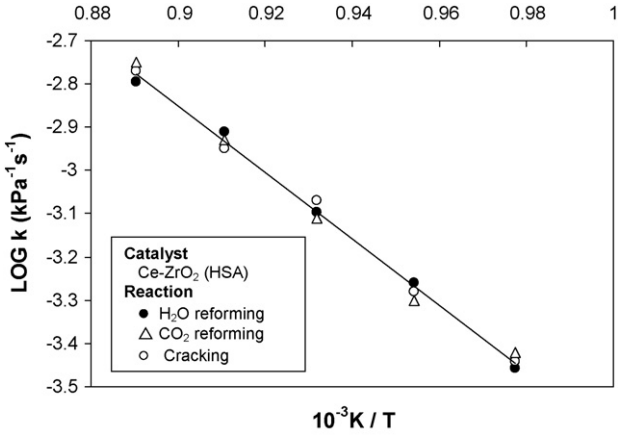

Fig. 8. Arrhenius plots for H_2O reforming, CO_2 reforming and cracking of CH_4 over Ce-ZrO_2 (HSA).

at each reaction temperature, Table 3. The activation energies for these three reactions, achieved by the Arrhenius plots as shown in Fig. 8, were between 150 and 155 kJ mol^{-1}, which are in good agreement with the values previously reported [9–10]. Due to the identical CH_4 reaction rates, the reaction order in CH_4, the rate constants, and the activation energies for all H_2O reforming, CO_2 reforming and cracking of CH_4, it could be concluded that all three reactions over ceria-based materials have similar reaction pathways in CH_4 activity.

3.4. Reactivity toward reforming and decomposition of oxyhydrocarbon

The decompositions of CH_3OH with and without co-reactant elements (i.e. H_2O and CO_2) were studied to confirm the above redox mechanism. The feed condition was co-reactant/CH_3OH in helium with the several molar ratios in the temperature range of 873–1073 K (to prevent the influence of homogeneous non-catalytic reaction). It should be noted according to our experimental results that, similar to CH_4 reforming, the reaction rate (per degree of OSC) and the kinetic dependencies of CH_3OH reaction rates were identical for all ceria-based materials, except the requirement of inlet co-reactant partial pressure to operate without detectable carbon formation. We thereby report here detailed reactivity and kinetic data only on Ce-ZrO_2 (HSA) sample.

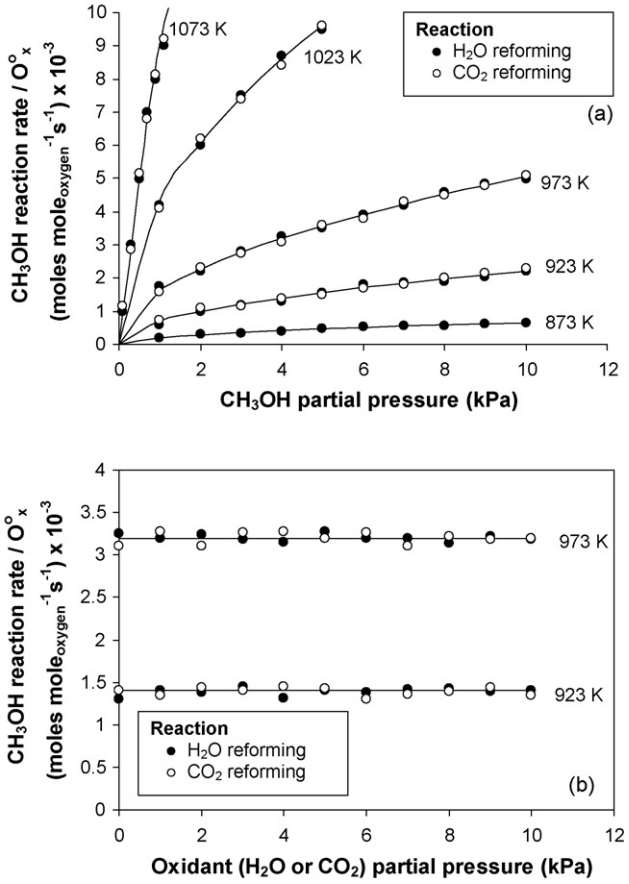

Fig. 9. Effects of CH_3OH partial pressure (a) and co-reactant partial pressure (b) on CH_3OH reaction rate (per moles of oxygen stored) over Ce-ZrO_2 (HSA).

After operation for 10 h, the main products from the reaction were H_2, CO, and CO_2, with small amount of CH_4 depending on the operating conditions, Table 4. According to the TPO, no carbon formation was observed in all studies. The effects of CH_3OH, H_2O, CO_2, CO and H_2 partial pressures on the rate was then studied by varying inlet CH_3OH partial pressure from 1 to 10 kPa (Fig. 9a) and changing the inlet co-reactant (H_2O or CO_2) partial pressure from 0 to 10 kPa (while keeping CH_3OH partial pressure constant at 4 kPa) (Fig. 9b). The results show that the reaction rate was proportional to CH_3OH concentration with the reaction order of 0.50 (±0.04). The rate was unaffected by H_2O and CO_2 partial pressures, in contrast, it was inhibited by the presence of H_2 and CO in the feed. The reaction orders in

Table 4
Reaction rate and fraction of by-products from the H_2O reforming of CH_3OH on Ce-ZrO_2 (HSA) at several temperature and various inlet H_2O/CH_3OH ratios (3 kPa CH_3OH balance in He)

Temperature (K)	H_2O/CH_3OH ratio	CH_3OH reaction rate/$O_O{}^x$ (moles $mole^{-1}_{oxygen}$ s^{-1}) × 10^{-3}	Yield of H_2 production (%)	Fraction of by-products (%)		
				CO	CO_2	CH_4
923	0.0	1.21	24.5	46.6	17.5	35.9
973	0.0	2.77	34.9	68.1	16.7	15.2
1023	0.0	7.45	42.8	85.1	14.9	0
1023	1.0	7.44	44.1	77.2	22.8	0
1023	2.0	7.46	45.9	70.3	29.7	0
1023	3.0	7.42	47.7	64.2	35.8	0

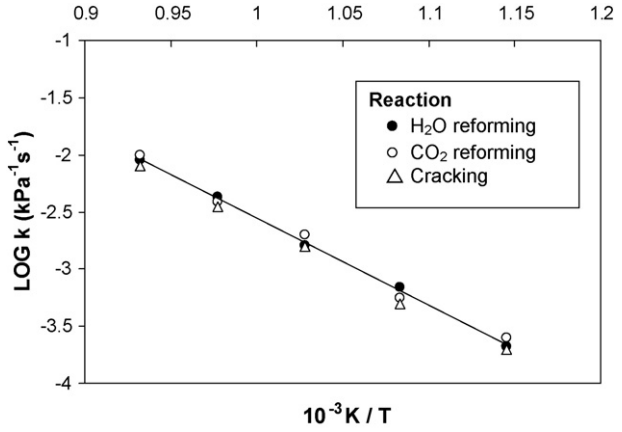

Fig. 10. Arrhenius plots for H_2O reforming, CO_2 reforming and cracking of CH_3OH over Ce-ZrO_2 (HSA).

H_2 and CO were between −0.28 (±0.01) and −0.13 (±0.02), respectively. The activation energies for H_2O reforming, CO_2 reforming and cracking of CH_3OH, achieved by the Arrhenius plots (Fig. 10), were 150–155 kJ/mol, which are closed to those observed from the CH_4 reactions. Therefore, based on the redox mechanistic proposal for CH_4 reaction, we suggested that the CH_3OH reaction mechanism over ceria-based materials could be written as followings:

$$CH_3OH + 2* \rightarrow CH_3* + OH* \quad (23)$$

$$CH_3* + 3* \rightarrow C* + 3H* \quad (24)$$

$$C* + O_O{}^x \rightarrow CO* + V_O{}^{\bullet\bullet} + 2e' \quad (25)$$

$$OH* + * \Leftrightarrow H* + O* \quad (26)$$

$$V_O{}^{\bullet\bullet} + 2e' + O* \Leftrightarrow O_O{}^x + * \quad (27)$$

CH_3OH first adsorbed on * forming intermediate surface hydrocarbon species (CH_x*) and OH* (Eq. (23)). Similar to CH_4 reforming, the intermediate surface hydrocarbons then adsorbed on the active surface site and reacted with the lattice oxygen ($O_O{}^x$) (Eqs. (24) and (25)). The steady-state reforming rate is due to the continuous supply of the oxygen containing compounds present in the system (i.e. H_2O, CO_2 and also CH_3OH) to regenerate the lattice oxygen ($O_O{}^x$). The dependence of the CH_3OH decomposition rate on CH_3OH partial pressure without the co-reactant requirement and its independence of the co-reactant partial pressures indicate that the lattice oxygen ($O_O{}^x$) is replenished by a sufficiently rapid reaction of the partially reduced state with the oxygen containing molecules in CH_3OH. The unchanged state of material was also confirmed by the calculation of oxygen balance during reactions and TPO after reactions.

The capability to decompose CH_3OH without requirement of steam is the great advantage of ceria-based materials for applying in SOFC system. Without the presence of steam being required, the consideration of water management in SOFC system is negligible and it is expected to simplify the overall SOFC system design, making SOFC more attractive to be used commercially.

3.5. Reactivity toward the high hydrocarbons (C_2H_4, C_2H_6, and C_3H_8) reforming

We again report here details only on Ce-ZrO_2 (HSA) sample, as the kinetic dependencies for these hydrocarbons were identical for all ceria-based materials. The feed was hydrocarbon (either C_2H_4, C_2H_6, or C_3H_8) and co-reactant (either H_2O or CO_2) in He. Catalyst reactivity and the product selectivities are given in Table 5. At 923 K, the main products from the reforming reactions were CH_4, H_2 CO, and CO_2. The formation of C_2H_4 was also observed toward the reforming of C_3H_8 and C_2H_6. From the studies, H_2 and CO selectivities increased with increasing temperature, whereas CO_2 and C_2H_4 selectivities decreased. The dependence of CH_4 selectivity on the operating temperature was non-monotonic; maximum CH_4 production occurred at approximately 1073 K (43.8%, 30.6% and 23.5% from steam reforming of C_2H_4, C_2H_6, and C_3H_8, respectively). These observations are in good agreement with our previous work, which studied the effect of temperature on the steam reforming of ethanol, ethane and ethylene over CeO_2 [49]. The decreases in CH_4 and C_2H_4 selectivities at higher temperature could be due to the further reforming to generate more CO and H_2. From the TPO testing, the amount of carbon deposited decreased with increasing inlet co-reactant concentration. At H_2O/hydrocarbons molar ratio higher than 3.0 and CO_2/hydrocarbons molar ratio higher than 5.0, no carbon formation was detected on the surface of Ce-ZrO_2 (HSA).

The influences of inlet component partial pressures on the reaction rate were then studied under the operating conditions without detectable carbon formation by changing the inlet

Table 5
Reaction rate and fraction of by-products from the H_2O and CO_2 reforming of C_nH_m on Ce-ZrO_2 (HSA) (923 K, 3 kPa C_nH_m and 15 kPa co-reactant, balance in He)

Reactant	Co-reactant	C_nH_m reaction rate/$O_O{}^x$	Yield of H_2 production (%)	Fraction of by-products (%)				Activation energy (kJ mol^{-1})
				C_2H_4	CH_4	CO	CO_2	
C_2H_4	H_2O	2.04[a]	26.7	–	40	48.2	11.8	150.4
	CO_2	2.10	15.5					151.9
C_2H_6	H_2O	2.85	29.9	9.3	28.6	49.2	12.9	148.6
	CO_2	2.78	18.4					147.5
C_3H_8	H_2O	5.39	34.3	18.6	20.3	48.5	12.6	145.0
	CO_2	5.44	22.1					149.7

[a] (moles $mole^{-1}_{oxygen}$ s^{-1}) × 10^{-3}.

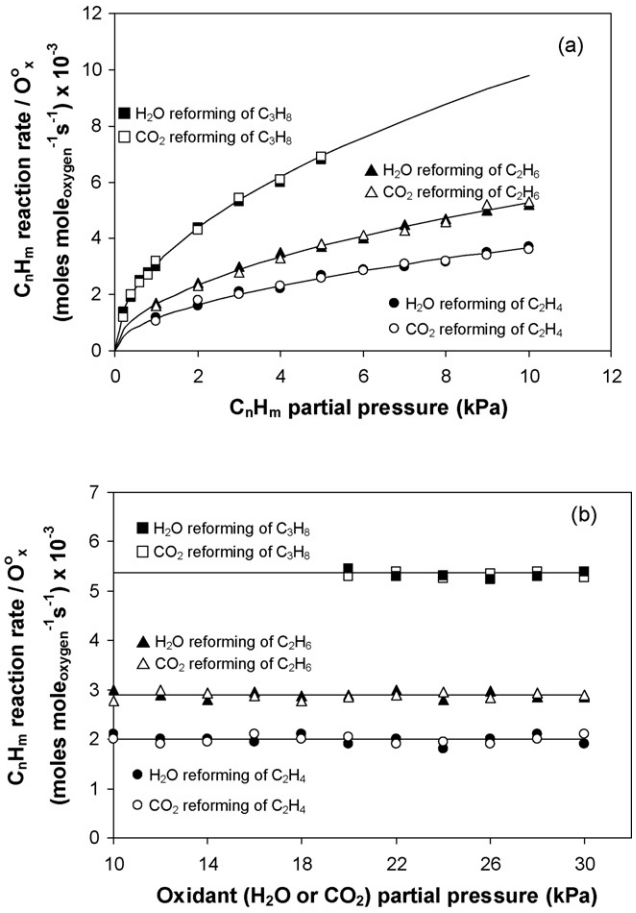

Fig. 11. Effects of C_nH_m partial pressures (a) and co-reactant partial pressure (b) on C_nH_m reaction rate (per moles of oxygen stored) over Ce-ZrO_2 (HSA) at 923 K.

hydrocarbon and co-reactant partial pressures as represented in Fig. 11a and b. Similar trends as CH_4 and CH_3OH reforming were observed. The reforming rate was proportional to the hydrocarbons concentration with the reaction orders in all hydrocarbons between 0.53 and 0.55. The rate was independent of inlet H_2O and CO_2 partial pressures, but it was inhibited by the presence of H_2 and CO in the feed. Fig. 12 shows the

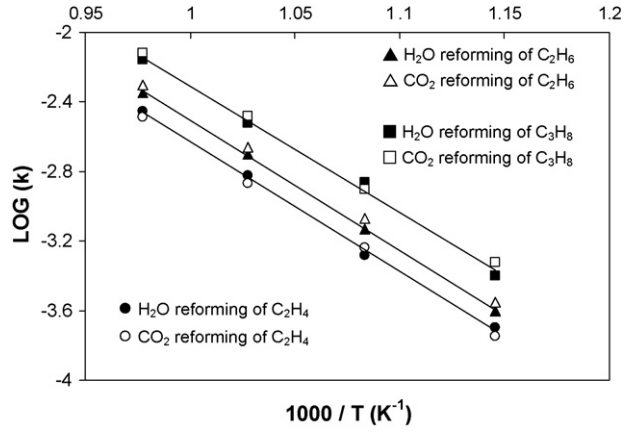

Fig. 12. Arrhenius plots for H_2O and CO_2 reforming of C_nH_m over Ce-ZrO_2 (HSA).

Arrhenius plots for both H_2O and CO_2 reforming of C_nH_m over Ce-ZrO_2 (HSA). The observed activation energies for these C_nH_m reactions were in the same range as achieved from the CH_4 and CH_3OH reactions (145–152 kJ mol^{-1}). Therefore, it can also be summarized that the mechanisms for H_2O and CO_2 reforming of high hydrocarbon are almost similar to those of CH_4 except that the adsorptions of these hydrocarbon elements (Eqs. (28–30)) are applied instead of the CH_4 adsorption. In addition, the reforming of high hydrocarbons requires considerably higher content of co-reactant at the feed in order to operate properly without the problem of carbon deposition.

$$C_3H_8 + 3* \rightarrow 2(CH_3*) + CH_2* \quad (28)$$

$$C_2H_6 + 2* \rightarrow 2CH_3* \quad (29)$$

$$C_2H_4 + 2* \rightarrow 7CH_2* \quad (30)$$

The capability to reform high hydrocarbon compounds with excellent resistance toward carbon deposition is another great benefit of ceria-based catalysts. Currently, natural gas and liquid petroleum gas (LPG) are the most promising primary fuels for the production of H_2 via reforming process. In order to reform these fuels, either an external pre-reforming unit or expensive noble metal catalysts (i.e. Rh) is normally required. By applying high surface area ceria-based materials as the reforming catalyst, all hydrocarbon elements can be reformed properly without the problem of carbon deposition eliminating the requirements of these costly processes.

4. Conclusion

High surface area CeO_2 and Ce-ZrO_2 provided higher CH_4, C_2H_4, C_2H_6, C_3H_8 and CH_3OH reforming rates with greater resistance toward carbon deposition than conventional Ce-ZrO_2 and CeO_2. The rates per amount of oxygen stored (moles mol^{-1}_{Oxygen} s^{-1}) on the surface of all ceria sample were in the same range, indicating the linear influence of OSC on the reaction rates. The kinetic dependencies of hydrocarbon conversions and the activation energies over these ceria-based materials were unaffected by the material specific surface area, doping element, degree of OSC and reactions. The rates were proportional to hydrocarbon partial pressures with positive fraction reaction order; independent of co-reactant partial pressures; but inhibited by CO and H_2. A set of unifying redox mechanistic proposal, in which the sole relevant elementary step is the reaction of intermediate surface hydrocarbon species with the lattice oxygen (O_O^x) and that oxygen is efficiently replenished by a rapid surface reaction with oxygen source in the system, was applied to explain these observed kinetic dependencies.

The capabilities to decompose oxyhydrocarbons without the requirement of steam and reform high hydrocarbon compounds with excellent resistance toward carbon deposition are the great benefit of ceria-based catalysts particularly for applying in SOFC system. Without the presence of steam being required, the consideration of water management in SOFC system is negligible, while the capability to reform high hydrocarbon

compounds with excellent resistance toward carbon deposition eliminates the requirement of expensive noble metal catalysts or the installation of external pre-reformer. These benefits simplify the overall SOFC system design, making SOFC more attractive for commercial uses.

Acknowledgements

The financial support from The Thailand Research Fund (TRF) throughout this project is gratefully acknowledged.

References

[1] A. Trovarelli, Catal. Rev. -Sci. Eng. 38 (1996) 439.
[2] P. Fornasiero, G. Balducci, R.D. Monte, J. Kaspar, V. Sergo, G. Gubitosa, A. Ferrero, M. Graziani, J. Catal. 164 (1996) 173.
[3] T. Miki, T. Ogawa, M. Haneda, N. Kakuta, A. Ueno, S. Tateishi, S. Matsuura, M. Sato, J. Phys. Chem. 94 (1990) 339.
[4] C. Padeste, N.W. Cant, D.L. Trimm, Catal. Lett. 18 (1993) 305.
[5] S. Kacimi, J. Barbier Jr., R. Taha, D. Duprez, Catal. Lett. 22 (1993) 343.
[6] G.S. Zafiris, R.J. Gorte, J. Catal. 143 (1993) 86.
[7] G.S. Zafiris, R.J. Gorte, J. Catal. 139 (1993) 561.
[8] S. Imamura, M. Shono, N. Okamoto, R. Hamada, S. Ishida, Appl. Catal. A 142 (1996) 279.
[9] E. Ramírez-Cabrera, A. Atkinson, D. Chadwick, Appl. Catal. B 47 (2004) 127.
[10] E. Ramírez-Cabrera, N. Laosiripojana, A. Atkinson, D. Chadwick, Catal. Today 78 (2003) 433.
[11] R.J. Gorte, J.M. Vohs, S. McIntosh, Solid State Ionics 175 (2004) 1.
[12] S. Jung, C. Lu, H. He, K. Ahn, R.J. Gorte, J.M. Vohs, J. Power Sources 154 (1) (2006) 42.
[13] T. Kim, G. Liu, M. Boaro, S.-I. Lee, J.M. Vohs, R.J. Gorte, O.H. Al-Madhi, B.O. Dabbousi, J. Power Sources 155 (2) (2006) 231.
[14] O. Costa-Nunes, R.J. Gorte, J.M. Vohs, J. Power Sources 141 (2005) 241.
[15] S. An, C. Lu, W.L. Worrell, R.J. Gorte, J.M. Vohs, Solid State Ionics 175 (2004) 135.
[16] D.J.L. Brett, A. Atkinson, D. Cumming, E. Ramírez-Cabrera, R. Rudkin, N.P. Brandon, Chem. Eng. Sci. 60 (2005) 5649.
[17] K. Otsuka, M. Hatano, A. Morikawa, J. Catal. 79 (1983) 493.
[18] K. Otsuka, M. Hatano, A. Morikawa, Inorg. Chim. Acta 109 (1985) 193.
[19] P.J. Gellings, H.J.M. Bouwmeester, Catal. Today 58 (2000) 1.
[20] D. Terribile, A. Trovarelli, J. Llorca, C. Leitenburg, G. Dolcetti, J. Catal. 178 (1998) 299.
[21] E. Abi-aad, R. Bechara, J. Grimblot, A. Aboukaïs, Chem. Mater. 5 (1993) 793.
[22] L.A. Bruce, M. Hoang, A.E. Hughes, T.W. Turney, Appl. Catal. A 134 (1996) 351.
[23] P.L. Chen, I.W. Chen, J. Am. Ceram. Soc. 76 (1993) 1577.
[24] H.K. Varma, P. Mukundam, K.G.K. Warrier, A.D. Damodaran, J. Mater. Sci. Lett. 10 (1991) 666.
[25] M. Hirano, E. Kato, J. Am. Ceram. Soc. 79 (1996) 777.
[26] M. Vallet-Regi, F. Conde, S. Nicolopoulos, C.V. Ragel, J.M. Gonzales-Calbet, Mater. Sci. Forum 235–238 (1997) 291.
[27] A. Tschöpe, J.Y. Ying, NanoStruct. Mater. 4 (1994) 617.
[28] M. Pijolat, J.P. Viricelle, M. Soustelle, Stud. Surf. Sci. Catal. 91 (1995) 885.
[29] T. Masui, K. Fujiwara, K. Machida, G. Adachi, T. Sakata, H. Mori, Chem. Mater. 9 (1997) 2197.
[30] Y. Zhou, R.J. Phillips, J.A. Switzer, J. Am. Ceram. Soc. 78 (1995) 981.
[31] V. Perrichon, A. Laachir, S. Abouarnadasse, O. Touret, G. Blanchard, Appl. Catal. A 129 (1995) 69.
[32] D. Terribile, A. Trovarelli, J. Llorca, C. Leitenburg, G. Dolcetti, Catal. Today 43 (1998) 79.
[33] M. Ozawa, M. Kimura, A. Isogai, J. Alloys Comp. 193 (1993) 73.
[34] G. Balducci, J. Kaspar, P. Fornasiero, M. Graziani, M.S. Islam, J. Phys. Chem. B 102 (1998) 557.
[35] G. Vlaic, P. Fornasiero, S. Geremia, J. Kaspar, M. Graziani, J. Catal. 168 (1997) 386.
[36] G.R. Rao, J. Kaspar, S. Meriani, R. Dimonte, M. Graziani, Catal. Lett. 24 (1994) 107.
[37] P. Fornasiero, R. Dimonte, G.R. Rao, J. Kaspar, S. Meriani, A. Trovarelli, M. Graziani, J. Catal. 151 (1995) 168.
[38] M.H. Yao, T.E. Hoost, R.J. Baird, F.W. Kunz, J. Catal. 166 (1997) 67.
[39] D. Kim, J. Am. Ceram. Soc. 72 (1989) 1415.
[40] N. Laosiripojana, W. Sutthisripok, S. Assabumrungrat, Chem. Eng. J. 127 (13) (2007) 36.
[41] N. Kruse, A. Frennet, J.M. Bastin (Eds.), Catalysis and Automotive Pollution Control IV, Elsevier, Amsterdam, 1998.
[42] J. Kaspar, P. Fornasiero, M. Graziani, Catal. Today 50 (1999) 285.
[43] H.S. Roh, H.S. Potdar, K.W. Jun, Catal. Today 93–95 (2004) 39.
[44] J. Wei, E. Iglesia, J. Catal. 225 (2004) 116.
[45] N. Laosiripojana, S. Assabumrungrat, Appl. Catal. A 290 (2005) 200.
[46] N. Laosiripojana, S. Assabumrungrat, Appl. Catal. B 60 (2005) 107.
[47] Y. Lwin, W.R.W. Daud, A.B. Mohamad, Z. Yaakob, Int. J. Hydrogen Energy 25 (2000) 47.
[48] J.N. Amor, Appl. Catal. A 176 (1999) 159.
[49] N. Laosiripojana, S. Assabumrungrat, Appl. Catal. B 66 (2006) 29.